atmosphere

MDPI

Article

Ionospheric Variability during the 2020–2021 SSW: COSMIC-2 Observations and WACCM-X Simulations

Nicholas Pedatella [1,2]

[1] High Altitude Observatory, National Center for Atmospheric Research, Boulder, CO 80307, USA; nickp@ucar.edu
[2] COSMIC Program Office, University Corporation for Atmospheric Research, Boulder, CO 80307, USA

Abstract: Variability in the ionosphere during the 2020–2021 sudden stratospheric warming (SSW) is investigated using a combination of Constellation Observing System for Meteorology, Ionosphere, and Climate-2 (COSMIC-2) observations and the Whole Atmosphere Community Climate Model with thermosphere–ionosphere eXtension (WACCM-X) simulations. The unprecedented spatial–temporal sampling of the low latitude ionosphere afforded by COSMIC-2 enables investigating the short-term (<5 days) variability in the ionosphere during the SSW event. The COSMIC-2 observations reveal a reduction in the diurnal and zonal mean ionosphere total electron content (ITEC) and reduced amplitude of the diurnal variation in the ionosphere during the SSW. Enhanced ITEC amplitudes of the semidiurnal solar and lunar migrating tides and the westward propagating semidiurnal tide with zonal wavenumber 3 are also observed. The WACCM-X simulations demonstrate that these variations are driven by variability in the stratosphere–mesosphere during the 2020–2021 SSW event. The results show the impact of the 2020–2021 SSW on the mean state, diurnal, and semidiurnal variations in the ionosphere, as well as the capabilities of the COSMIC-2 mission to observe short-term variability in the ionosphere that is driven by meteorological variability in the lower atmosphere.

Keywords: COSMIC-2; ionosphere; sudden stratosphere warming

Citation: Pedatella, N. Ionospheric Variability during the 2020–2021 SSW: COSMIC-2 Observations and WACCM-X Simulations. *Atmosphere* **2022**, *13*, 368. https://doi.org/10.3390/atmos13030368

Academic Editor:Alexei Dmitriev

Received: 24 January 2022
Accepted: 17 February 2022
Published: 22 February 2022

1. Introduction

Sudden stratospheric warmings (SSWs) are large-scale meteorological events that are driven by the dissipation of planetary waves propagating upwards from the troposphere [1]. SSW events are identified based on the changes that occur in the stratosphere, including a rapid increase in polar temperatures and a deceleration of the zonal mean zonal winds. A SSW is classified as a major SSW if the zonal mean zonal winds at 60° N and 10 hPa reverse from eastward to westward and is considered minor if the winds remain eastward for the duration of the event [2]. Although SSWs were originally identified and characterized by changes in stratospheric dynamics, it is now recognized that they lead to disturbances throughout the entire atmosphere. This includes altering tropospheric weather patterns, chemistry and dynamics of the stratosphere–mesosphere, and the composition, dynamics, and electrodynamics of the ionosphere–thermosphere [3,4].

Though originally hypothesized by Stening [5], the influence of SSWs on the upper atmosphere (ionosphere–thermosphere) attracted significant attention following the studies of Goncharenko and Zhang [6], Chau et al. [7], and Goncharenko et al. [8], who clearly identified the impacts of SSWs on ion temperatures, equatorial vertical drift, and total electron content (TEC), respectively. The focus on SSWs is, at least in part, due to the fact that they represent an identifiable forcing mechanism that can be used to understand coupling mechanisms between the lower and upper atmospheres. Subsequent studies further demonstrated the broad extent to which SSWs influence the ionosphere–thermosphere. This includes impacts on electron densities at both low and middle latitudes, equatorial electrodynamics, small-scale irregularities (i.e., scintillation and traveling ionosphere disturbances), and thermosphere density and composition (see reviews by [9,10]). The SSW

induced variability in the ionosphere–thermosphere is ultimately driven by the changes that occur in the stratosphere and mesosphere. Observational and modeling studies have demonstrated that the changes in the stratosphere influence the generation and propagation of solar and lunar tides [11–13]. Variability in the tides modifies the winds that drive the E-region dynamo, introducing variability in the electrodynamics that, in turn, influence the electron density e.g., [14]. Tidal dissipation also alters the residual mean circulation of the mesosphere and lower thermosphere (MLT), leading to changes in the thermosphere composition [15,16]. Changes in thermosphere composition during SSWs subsequently alter the mean state of the ionosphere [15].

Direct observations of the ionospheric variability during SSWs has been challenged by observational limitations, especially given the relatively short time scales that can be involved. While ground-based observations can clearly observe the day-to-day variations in the ionosphere that occur during SSWs e.g., [17], they are limited in their longitudinal coverage. This presents a considerable limitation to ground-based observations given the presence of longitudinal differences in the ionospheric response to SSWs [18–20]. Satellite observations can potentially address this issue, though, to date, they have lacked sufficient sampling to observe the ionospheric variability on short time scales. For example, Lin et al. [21] and Lin et al. [22] investigated the ionospheric variability during the 2009 SSW using the Constellation Observing System for Meteorology, Ionosphere, and Climate (COSMIC) observations. However, in order to obtain full longitude and local time sampling, it was necessary to average the results over 20 days, potentially missing the variability that occurred on shorter time scales.

The COSMIC-2 constellation samples the low latitude ionosphere with significantly greater density compared to previous satellite missions, giving an unprecedented view of the day-to-day ionospheric variability. Motivated by the dense sampling of the ionosphere made possible by COSMIC-2, the objective of the present study is to investigate the ionospheric variability during the 2020–2021 SSW. The 2020–2021 SSW occurred when the COSMIC-2 constellation was nearly in its operational configuration, providing among the first opportunities to leverage the density of COSMIC-2 observations to investigate the short-term variability of the ionosphere that is driven by meteorological variability. The COSMIC-2 observations are complemented by numerical simulations performed using the Whole Atmosphere Community Climate Model with thermosphere–ionosphere eXtension (WACCM-X). The WACCM-X simulations enable understanding of the sources of the ionosphere variability observed by COSMIC-2. The results illustrate the capabilities of the COSMIC-2 observations to capture the rapid variations that occur in the ionosphere during SSW events and demonstrate that the 2020–2021 SSW was associated with complex variability in the ionosphere that was driven by a combination of variability due to the SSW and from solar/geomagnetic activity.

2. Observations and Model Simulations

2.1. COSMIC-2 Observations

COSMIC-2 consists of six satellites that were launched into low Earth orbit on 25 June 2019. The COSMIC-2 satellites were initially launched into ∼720 km altitude 24° inclination parking orbits and were subsequently lowered to their operational orbits of ∼550 km [23]. By the time period that is the focus of this study (November 2020–March 2021), five of the six COSMIC-2 satellites were in their operational orbits. The final satellite (FM6) was lowered to its operational orbit altitude in January 2021, and no data are available from this satellite from 10 January to 3 February 2021. Each COSMIC-2 satellite has several payloads, including a Tri-GNSS Radio Occultation System (TGRS), Ion Velocity Meter (IVM), and Radio Frequency Beacon (RFB) [24]. The present study analyzes ionosphere electron density profiles that are derived from the TGRS line-of-sight Total Electron Content (TEC) observations using the Abel inversion [25,26].

The COSMIC-2 observations are analyzed as follows. The individual electron density profiles are vertically integrated up to ∼550 km to obtain the ionosphere TEC (ITEC).

Within a 5-day running window, the ITEC is binned in 2.5° magnetic latitude, 12° geographic longitude, and 1 h local time. The value in each bin is based on the median value of the observations after removal of any ITEC values that fall outside the range $\mathrm{ITEC}_{\mathrm{mean}} \pm 3 \times \mathrm{ITEC}_{\sigma}$, where $\mathrm{ITEC}_{\mathrm{mean}}$ and ITEC_{σ} are the mean and standard deviation of the ITEC values in each bin. The typical number of points within each bin is 4–8 between ±35° magnetic latitude, with greater sampling density between ±20° magnetic latitude. Poleward of ∼35° magnetic latitude, COSMIC-2 does not sample all longitudes, so the results are limited to ±35°. Following Lin et al. [21], the ITEC is then decomposed into the mean and the diurnal and semidiurnal migrating and nonmigrating tides:

$$\mathrm{ITEC}(t,\phi) = \overline{\mathrm{ITEC}} + \sum_{n=1}^{2} \sum_{s=n-5}^{n+5} A_{n,s} \cos[\frac{2\pi n}{24}\mathrm{LT}_{\mathrm{hr}} - (n+s)\lambda + \theta_{n,s}] \quad (1)$$

where t is time in days, ϕ is magnetic latitude, $\overline{\mathrm{ITEC}}$ is the zonal and diurnal mean ITEC, $\mathrm{LT}_{\mathrm{hr}}$ is the solar local time in hours, λ is longitude, n is subharmonic of a solar day, and s is the zonal wavenumber. Equation (1) is solved for $A_{n,s}$ and $\theta_{n,s}$ for each day, t, and latitude, ϕ. Although the tidal variability in the ionosphere does not fully map to variations in the tides in the neutral atmosphere, it can be used as a reasonable proxy for variability in the semidiurnal tides [27] and also provides insight into the changes occurring in the ionosphere during SSWs, e.g., [21,28,29]. Note that due to using a 5-day window, the semidiurnal tides will contain contributions from both solar and lunar components, since they cannot be fully separated when considering a short temporal window. Though they can be separated using a longer window, a 5-day window is used in the present study to illustrate the advantages of the COSMIC-2 sampling to observe variability on shorter time scales. The use of a shorter window does, however, mean that beating between the migrating semidiurnal solar tide (SW2) and migrating semidiurnal lunar tide (M2) occurs, leading to short-term variations in the SW2 amplitude [29].

2.2. WACCM-X Simulations

WACCM-X simulations are used for both comparison with the COSMIC-2 observations as well as for aiding in the interpretation of the observational results. WACCM-X is a whole atmosphere model that extends from the surface to the upper thermosphere (4.1×10^{-10} hPa, ∼500–700 km depending on solar activity). The simulations are performed using WACCM-X version 2.1, which is part of the Community Earth System Model version 2.1 [30]. The chemical, dynamical, and physical processes in the troposphere, stratosphere, mesosphere, and lower thermosphere are based on the Community Atmosphere Model version 4 [31] and WACCM version 4 [32]. The ionosphere–thermosphere processes in WACCM-X are largely adopted from the Thermosphere-Ionosphere-Electrodynamics General Circulation Model (TIE-GCM) [33]. This includes transport of O^+, self-consistent electrodynamics, and ion/electron energetics. The model resolution is 1.9° × 2.5° in latitude × longitude. The vertical resolution is ∼1–3 km in the troposphere–stratosphere and 0.25 scale heights above 0.96 hPa. A detailed description of WACCM-X is provided by Liu et al. [34], and initial validation can be found in Liu et al. [35].

To simulate the conditions during the 2020–2021 SSW event, the model meteorology in the lower atmosphere (troposphere–stratosphere) is constrained to the National Aeronautics and Space Administration (NASA) Modern-Era Retrospective analysis for Research and Applications version 2 (MERRA-2) reanalysis [36]. The constraint is applied using the specified dynamics (SD) approach described in Smith et al. [37] and consists of nudging the model dynamical fields to the MERRA-2 dynamical fields up to ∼50 km. The model is free-running (i.e., unconstrained) above ∼50 km. The SD-WACCM-X simulations account for the realistic, time-varying, solar and geomagnetic variability through parameterizations based on the F10.7 cm solar flux and K_p geomagnetic index. The F10.7 cm solar flux is used to specify the solar extreme ultraviolet (EUV) variability and its effects on the ionosphere–thermosphere [38]. K_p is used to parameterize the high-latitude convection [39] and auroral

precipitation [40]. Forcing of the migrating semidiurnal lunar tide is included following Pedatella et al. [41].

Two additional WACCM-X simulations were performed in order to separate the ionosphere variability that is driven by the 2020–2021 SSW from solar and geomagnetic variability and seasonal variations. An additional SD-WACCM-X simulation was performed using constant solar and geomagnetic forcing of F10.7 = 70 solar flux units (sfu, 1 sfu = 10^{-22} W m^{-2} Hz^{-1}) and a K_p of 0^+. This simulation, which will be referred to as SD-WACCM-X Constant Solar, allows for separation of the ionosphere variability that is driven by the lower atmosphere from the solar and geomagnetic variations that occurred during the 2020–2021 SSW time period. An additional simulation was performed using constant solar and geomagnetic forcing for a 10-member ensemble of free-running WACCM-X. The free-running WACCM-X simulations are unconstrained in the lower atmosphere, and the ensemble mean of the 10-member ensemble is used to isolate the seasonal variations. This simulation is subsequently referred to as the WACCM-X Constant Solar Ensemble Mean.

3. Results and Discussion

Figure 1 presents the meteorological and solar/geomagnetic activity that drove the ionospheric variations between November 2020 and March 2021. Focusing first on the meteorological variability, the zonal mean zonal winds at 60°N illustrated an abrupt reversal of the winds throughout the stratosphere–mesosphere in early January. The winds at 10 hPa reversed on day 5, indicating the onset of a major SSW. Following the wind reversal, the stratospheric winds remained weak for 30–35 days, with additional stratospheric wind reversals occurring around days 12–22 and 31–34. The prolonged weakening of the winds in the lower stratosphere was attributed to the persistent tropospheric wave forcing during January 2021 [42]. However, it was only the initial wind reversal in early January that was accompanied by a wind reversal throughout the middle atmosphere, and the winds in the upper stratosphere and mesosphere remained eastward during the later wind reversals. The geomagnetic and solar activity were variable throughout the 2020–2021 SSW. The K_p index (Figure 1b) exhibited periods of moderate activity, with K_p values exceeding four on several occasions. Though this does not represent significant geomagnetic activity, even minor to moderate variations in K_p can impact the ionosphere [43]. The F10.7 cm solar flux had a high of ∼110 sfu on day −32, and then steadily declined to ∼70 sfu around day 5, where it remained relatively constant for the remainder of the time period.

The response of the mean state of the ionosphere to the SSW and the solar/geomagnetic variability is shown in Figure 2, which shows the diurnal and zonal mean ITEC (i.e., $\overline{\text{ITEC}}$ in Equation (1)) from the COSMIC-2 observations and the different WACCM-X simulations. The COSMIC-2 observations exhibited enhanced $\overline{\text{ITEC}}$ around days −40 to −20, days −10 to 0, and after day 50. A relative minimum in $\overline{\text{ITEC}}$ was also observed beginning around day 0 and persisted for ∼20 days. These features were, for the most part, well reproduced in the SD-WACCM-X simulation, indicating the fidelity of the model to capture the variations in the ionosphere that occurred due to both the 2020–2021 SSW as well as those due to geomagnetic and solar activity. The different model simulations provide insight into the sources of the $\overline{\text{ITEC}}$ variations. The enhancements prior to the SSW onset were absent from the SD-WACCM-X Constant Solar simulation, indicating that these were driven by increased solar and geomagnetic activity. The increased $\overline{\text{ITEC}}$ beginning around day 50 was attributed to seasonal variations due to its presence in both the SD-WACCM-X Constant Solar and WACCM-X Constant Solar Ensemble Mean simulations. The relative minimum in $\overline{\text{ITEC}}$ that was observed by COSMIC-2 in early January coincided with the SSW onset and was also present in both the SD-WACCM-X and SD-WACCM-X Constant Solar simulations. Though the WACCM-X Constant Solar Ensemble Mean simulation showed an $\overline{\text{ITEC}}$ seasonal minimum occurred around this time, there was a clear shift in the timing of the minimum in the SD-WACCM-X Constant Solar simulation. In particular, the seasonal minimum in $\overline{\text{ITEC}}$ occurred in late December, while the minimum in the SD-WACCM-X Constant Solar simulation occurred ∼10–15 days later, coincident with the

SSW. This demonstrates that the $\overline{\text{ITEC}}$ minimum was not solely due to seasonal variability. Rather, the $\overline{\text{ITEC}}$ minimum was attributed to the occurrence of the SSW and was related to the altered residual circulation in the MLT during the SSW. This led to a decrease in thermosphere composition and electron density [15,16]. The observed minimum in the COSMIC-2 $\overline{\text{ITEC}}$ in early January was thus due to the SSW. It should, however, be noted that the SSW was not responsible for the entirety of the observed $\overline{\text{ITEC}}$ decrease due to the gradual decline in F10.7 in the month prior to the SSW onset, which also led to a reduction in the $\overline{\text{ITEC}}$.

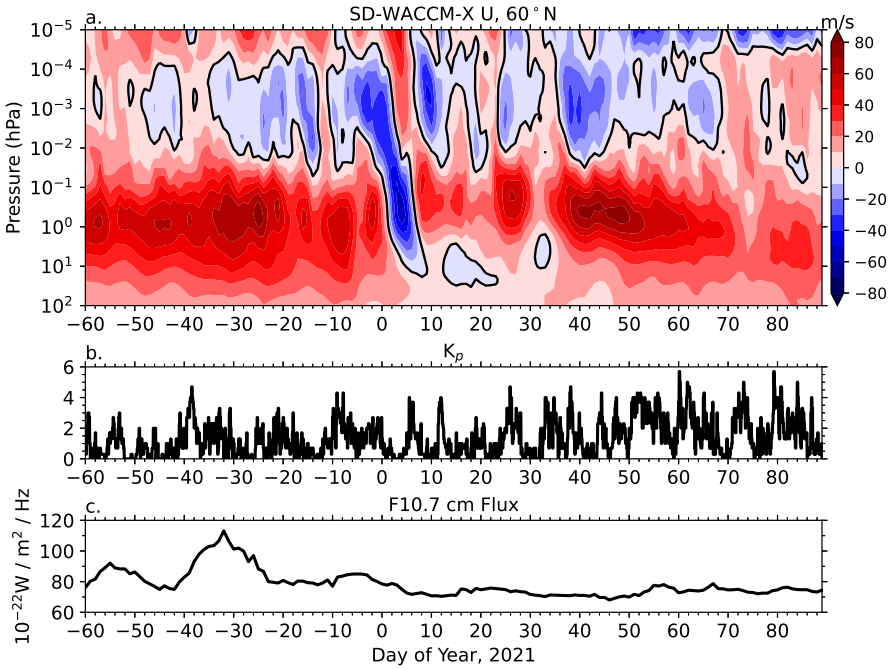

Figure 1. Variability in the (**a**) zonal mean zonal winds at 60°N from SD-WACCM-X, (**b**) geomagnetic K_p index, and (**c**) F10.7 cm solar flux during the 2020–2021 SSW.

We now turn our attention to the tidal variability during the 2020–2021 SSW, and its impact on the ionosphere. Figure 3 shows the variability in the diurnal migrating tide (DW1), semidiurnal migrating tide (SW2), and the westward propagating semidiurnal nonmigrating tides with zonal wavenumbers 1 (SW1) and 3 (SW3) in the MLT simulated by SD-WACCM-X. Note that as previously discussed, fitting for SW2 using a 5-day window will include a contribution from M2. The SW2 should thus be recognized as having contributions from both the SW2 and M2 tides, though it is referred to as SW2 in the remainder of the text. A number of different tidal modes exhibited variability during the the 2020–2021 SSW time period. Some of these variations may be due to nonlinear planetary wave tide interactions, e.g., [44,45], while others may be unrelated to the SSW (i.e., they arose due to internal atmospheric variability unrelated to the SSW). As the present study is focused on the ionosphere, we restrict our focus to the the DW1, SW2, SW1, and SW3 as these tides are known to exhibit a consistent response to SSWs and couple to the ionosphere [14,19,46–48]. The most pronounced variation in the tides during the 2020–2021 SSW was an enhancement in SW2, which was consistent with prior studies, e.g., [49]. Although previous studies have found a decrease in DW1 during some SSWs (e.g., 2009), the DW1 minimum during the 2020–2021 SSW occurred in early to middle December and was largely attributed to the seasonal variation in the DW1 [50]. SW2 was drastically enhanced in both hemispheres beginning around day 0, coincident with the wind reversal in the middle atmosphere. This initial enhancement lasted for ∼10 days, which was consistent with the timing of the wind reversal throughout the middle atmosphere. Subsequent enhancements in SW2 occurred primarily in the Northern Hemisphere around days 14–22 and 26–34. The timing of these enhancements coincided with periods of weaker

winds in the stratosphere–mesosphere (Figure 1a), indicating that they were likely related to enhanced propagation conditions [11]. Additionally, there was an evident periodicity to the SW2 amplitudes, with a period of ∼14 days that was attributed to the influence of M2 and the inability to separate the SW2 and M2 with a 5-day window. Notable variations were also seen in the SW1 and SW3, with several periods of enhanced amplitudes occurring throughout the 2020–2021 SSW time period. These enhancements often, though not always, corresponded to decreases in the SW2 amplitude suggesting that they may be due to nonlinear interactions between the SW2 and the quasi-stationary planetary wave with zonal wavenumber 1 (PW1) [51,52].

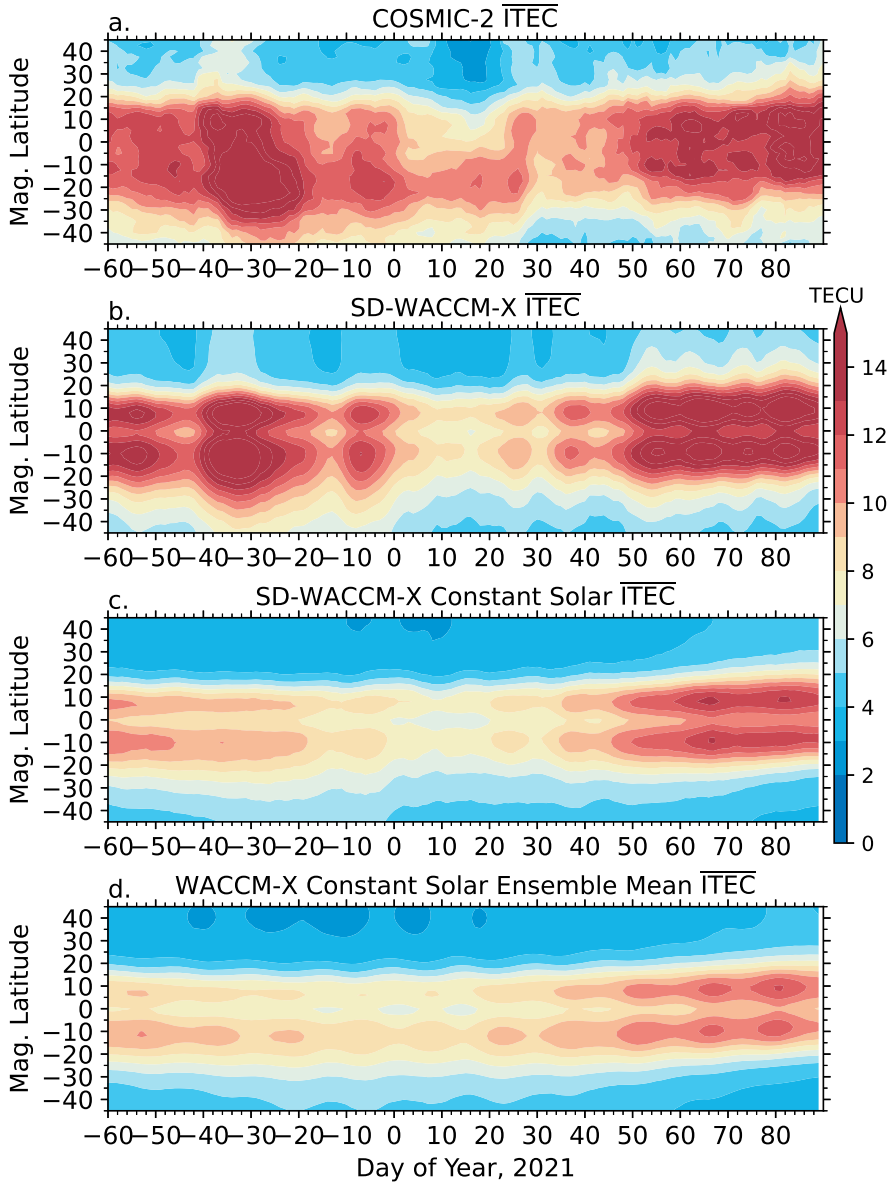

Figure 2. Diurnal and zonal mean ITEC ($\overline{\text{ITEC}}$) from (**a**) COSMIC-2 observations, (**b**) SD-WACCM-X, (**c**) SD-WACCM-X Constant Solar, and (**d**) WACCM-X Constant Solar Ensemble Mean.

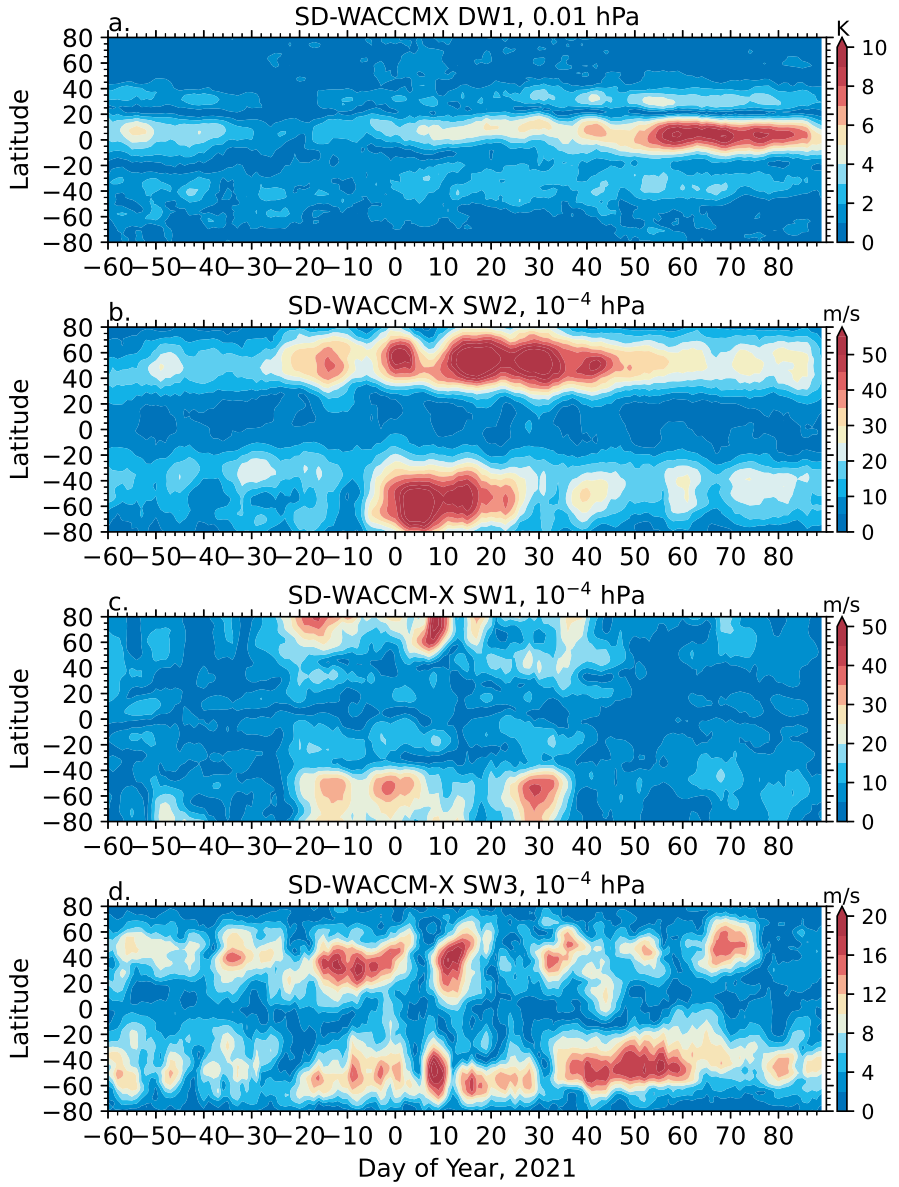

Figure 3. SD-WACCM-X amplitudes of the (**a**) DW1 at 0.01 hPa in temperature, (**b**) SW2 at 10^{-4} hPa in zonal wind, (**c**) SW1 at 10^{-4} hPa in zonal wind, and (**d**) SW3 at 10^{-4} hPa in zonal wind.

Figures 4–7 show the corresponding behavior of the tides in ITEC based on COSMIC-2 observations and WACCM-X simulations. The ITEC DW1 variations closely followed the behavior of the $\overline{\text{ITEC}}$ (Figure 2) in both the observations and model simulations, with little relationship to the DW1 in the MLT. In particular, a notable reduction occurred in both the $\overline{\text{ITEC}}$ as well as the ITEC DW1 in early January. The reduction in the ITEC DW1 can be interpreted as a reduction in the diurnal amplitude (i.e., difference between daytime and nighttime electron densities) of the ionosphere. As previously discussed, this decrease in $\overline{\text{ITEC}}$ is due to the altered residual circulation in the middle atmosphere during the SSW. The correspondence between the $\overline{\text{ITEC}}$ and ITEC DW1 is consistent with the numerical experiments of Chang et al. [27], who demonstrated that the DW1 in the ionosphere closely follows the diurnal and zonal mean electron density, and that both are influenced by changes in the residual circulation due to tidal dissipation. Thus, although the ITEC DW1 was not directly driven by the DW1 in the MLT, it was indirectly impacted by the enhanced tidal dissipation in the MLT during SSW events that, in turn, altered the residual circulation and mean state of the ionosphere–thermosphere.

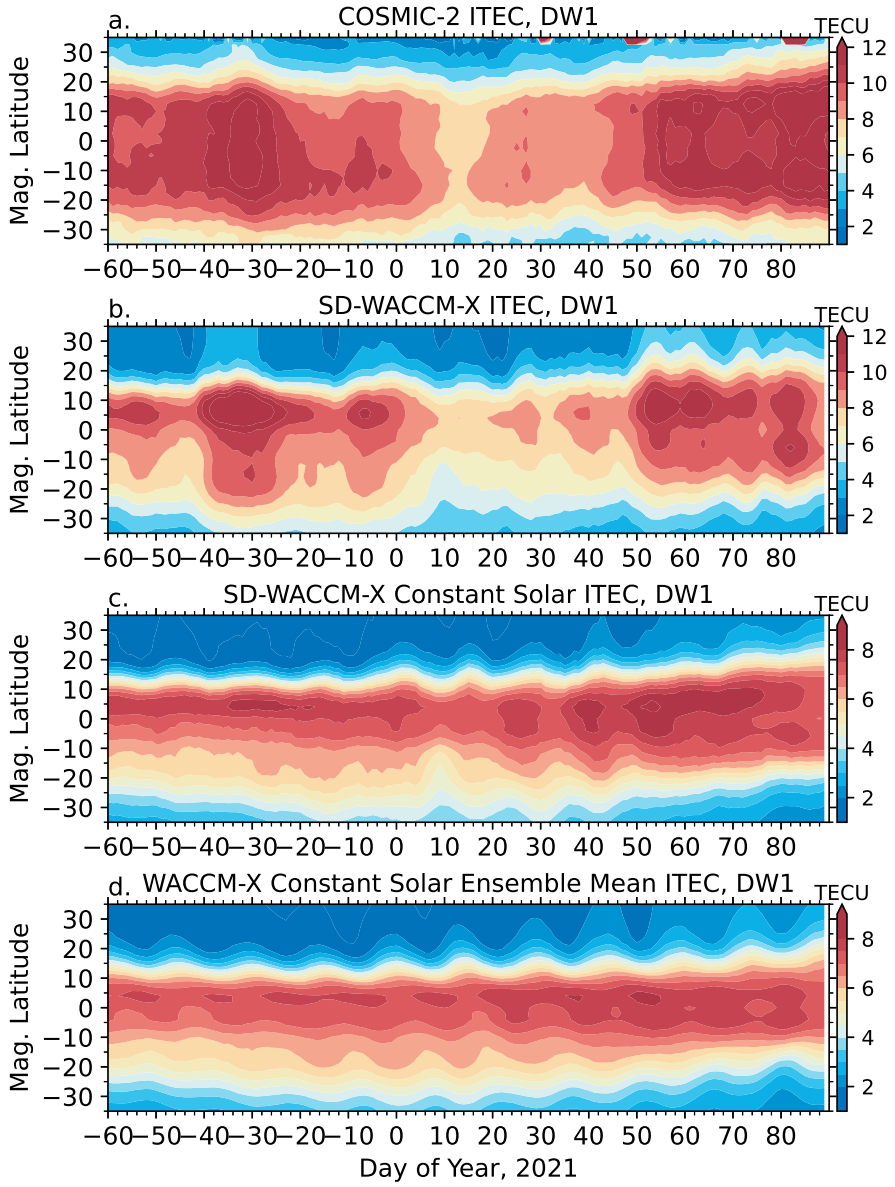

Figure 4. DW1 amplitude in ITEC from (**a**) COSMIC-2 observations, (**b**) SD-WACCM-X, (**c**) SD-WACCM-X Constant Solar, and (**d**) WACCM-X Constant Solar Ensemble Mean.

The ITEC SW2 showed notable oscillations throughout the entire time period of the 2020–2021 SSW event (Figure 5a–c). As previously discussed, the periodic behavior was related to the use of a 5-day window, which was unable to separate the semidiurnal solar and lunar tides leading to a ∼14-day oscillation in the SW2 [29]. The COSMIC-2 observations exhibited large amplitudes throughout nearly the entire period of November 2020 to March 2021. This differed from the SD-WACCM-X simulations, which showed enhanced ITEC SW2 amplitudes only between December 2020 and February 2021. However, both the SD-WACCM-X simulation and the COSMIC-2 observations demonstrated enhanced ITEC SW2 amplitudes occurring around days −30, 0, and 30. The enhancement occurring around day −30 was largely attributed to the enhanced solar activity at this time as it was not present in the SD-WACCM-X Constant Solar simulation. The enhanced ITEC SW2 amplitudes around days 0 and 30 were also present in the SD-WACCM-X Constant Solar simulation. Note that although the ITEC SW2 was slightly enhanced in early January in the WACCM-X Constant Solar Ensemble Mean simulation, the enhancement was greater in the SD-WACCM-X Constant Solar case demonstrating that these enhancements can be attributed to the SSW event. The timing of these enhancements was coincident with

enhanced SW2 amplitudes in the MLT (Figure 3b), indicating that they were likely due to the enhanced SW2 in the MLT modulating the E-region dynamo generation of electric fields [53,54].

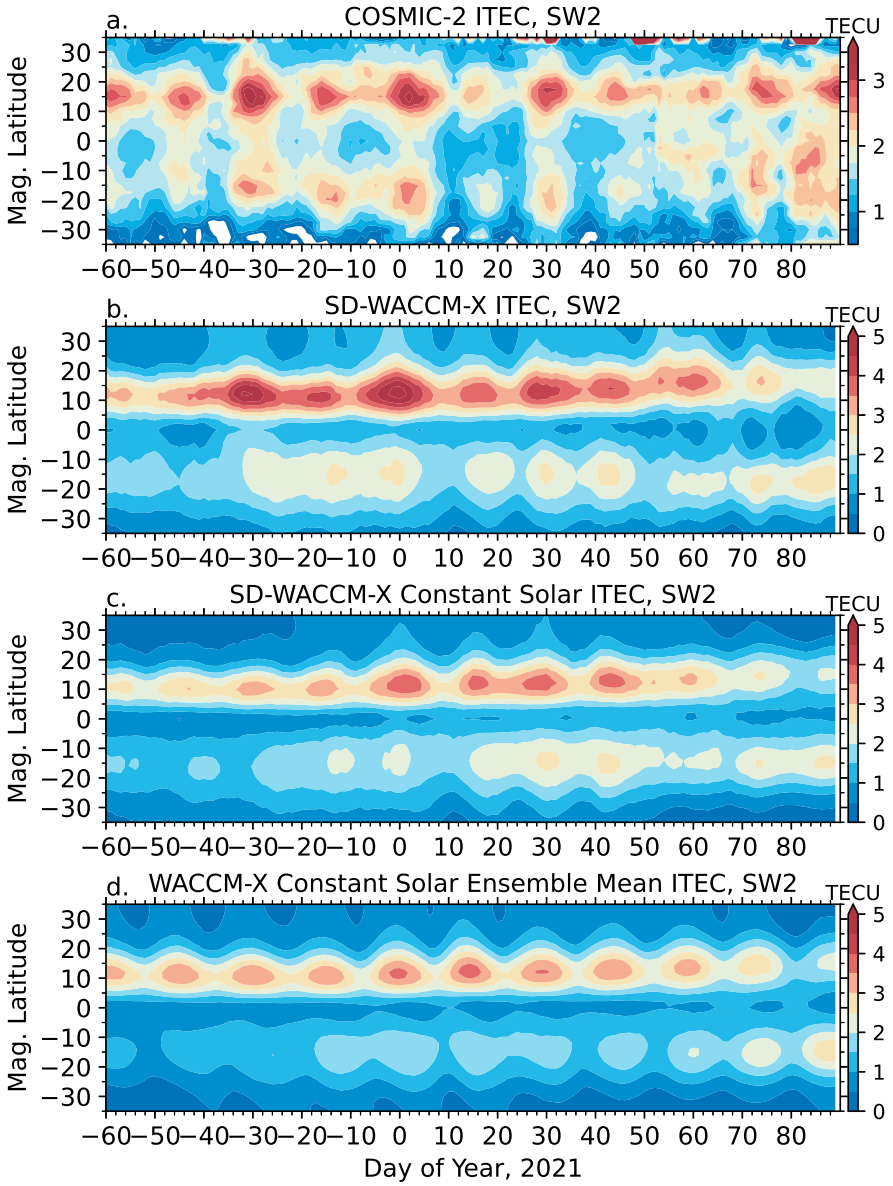

Figure 5. SW2 amplitude in ITEC from (**a**) COSMIC-2 observations, (**b**) SD-WACCM-X, (**c**) SD-WACCM-X Constant Solar, and (**d**) WACCM-X Constant Solar Ensemble Mean.

Last, we discuss the variability in the semidiurnal nonmigrating tides SW1 and SW3 (Figures 6 and 7). There is little agreement between the COSMIC-2 ITEC SW1 and the SD-WACCM-X ITEC SW1. Although the enhancements observed by COSMIC-2 around days −40 to −30, 40–60 and the periodic enhancements between days −20 and 20 also occurred in the SD-WACCM-X simulations, there were clear differences in the amplitudes of the enhancements and whether they occurred in the Northern or Southern Hemisphere. The SD-WACCM-X simulations also exhibited enhanced amplitudes that were not seen in the COSMIC-2 observations, especially in the Northern Hemisphere between days −30 and 40. A number of the enhancements seen in the simulations appeared to be driven by the lower atmospheric variability, as indicated by their presence in the SD-WACCM-X Constant Solar simulation. The enhanced ITEC SW1 amplitudes between roughly days −20 and 40 closely corresponded to enhanced SW1 amplitudes in the MLT (Figure 3c) indicating

that they were at least in part driven by the tidal variability. This would suggest that the COSMIC-2 ITEC SW1 were partly tidal driven, though this cannot be concluded with certainty owing to the lack of tidal observations and the disagreement between the model and observations. It should be noted that direct correspondence between SW1 in the MLT and ITEC may not be expected since the geomagnetic main field can introduce wavenumber 1 variations in the ionosphere, e.g., [14]. However, Maute et al. [52] demonstrated that the enhanced SW1 during SSWs is a significant contributor to the wavenumber 1 variations in the vertical drift. It is, thus, possible to attribute at least a portion of the ITEC SW1 to the enhanced tidal amplitudes in the MLT. Comparison of the observed and modeled ITEC SW3 (Figure 7) also showed considerable disagreement between the observations and SD-WACCM-X simulations. There was, however, clear agreement in the enhanced ITEC SW3 around the time of the SSW onset, with both the observations and simulations showing enhanced SW3 amplitudes around days −5 and 10. As indicated by their presence in the SD-WACCM-X Constant Solar simulation, these enhancements can be attributed to SSW related variability, and were likely driven by the enhanced SW3 amplitudes at MLT altitudes that occurred at the same time periods (Figure 3d).

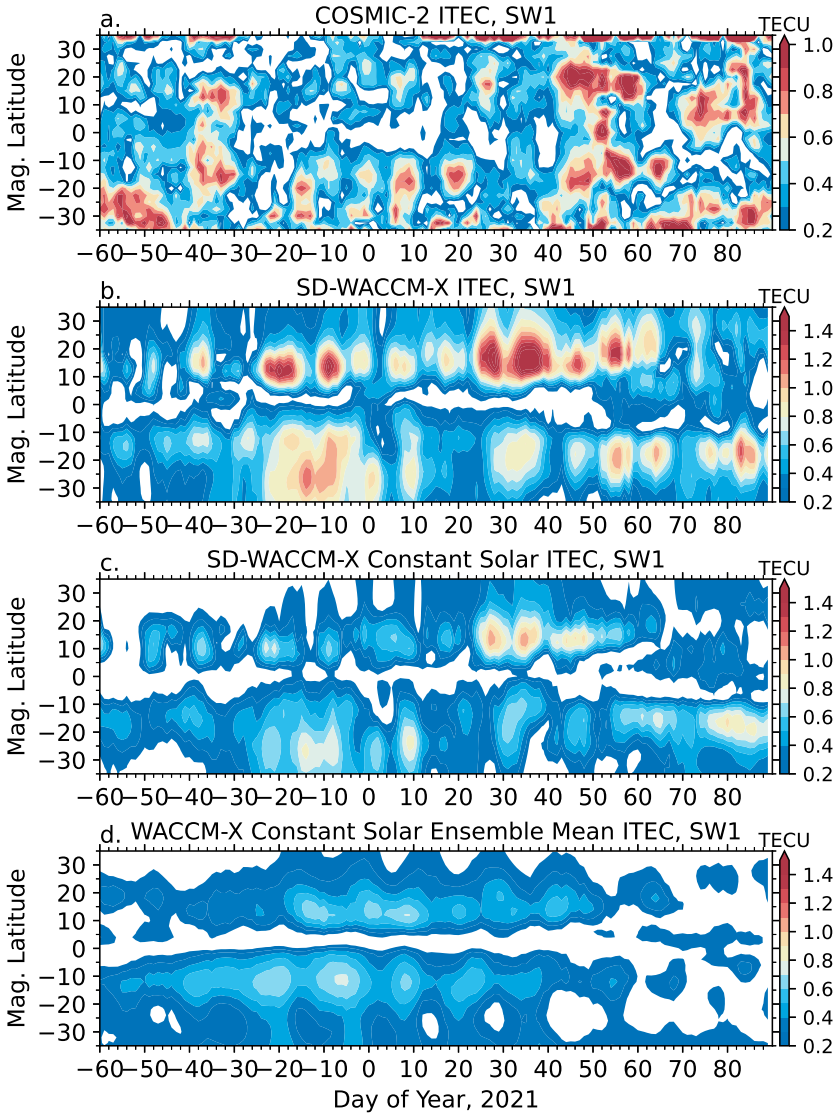

Figure 6. SW1 amplitude in ITEC from (**a**) COSMIC-2 observations, (**b**) SD-WACCM-X, (**c**) SD-WACCM-X Constant Solar, and (**d**) WACCM-X Constant Solar Ensemble Mean.

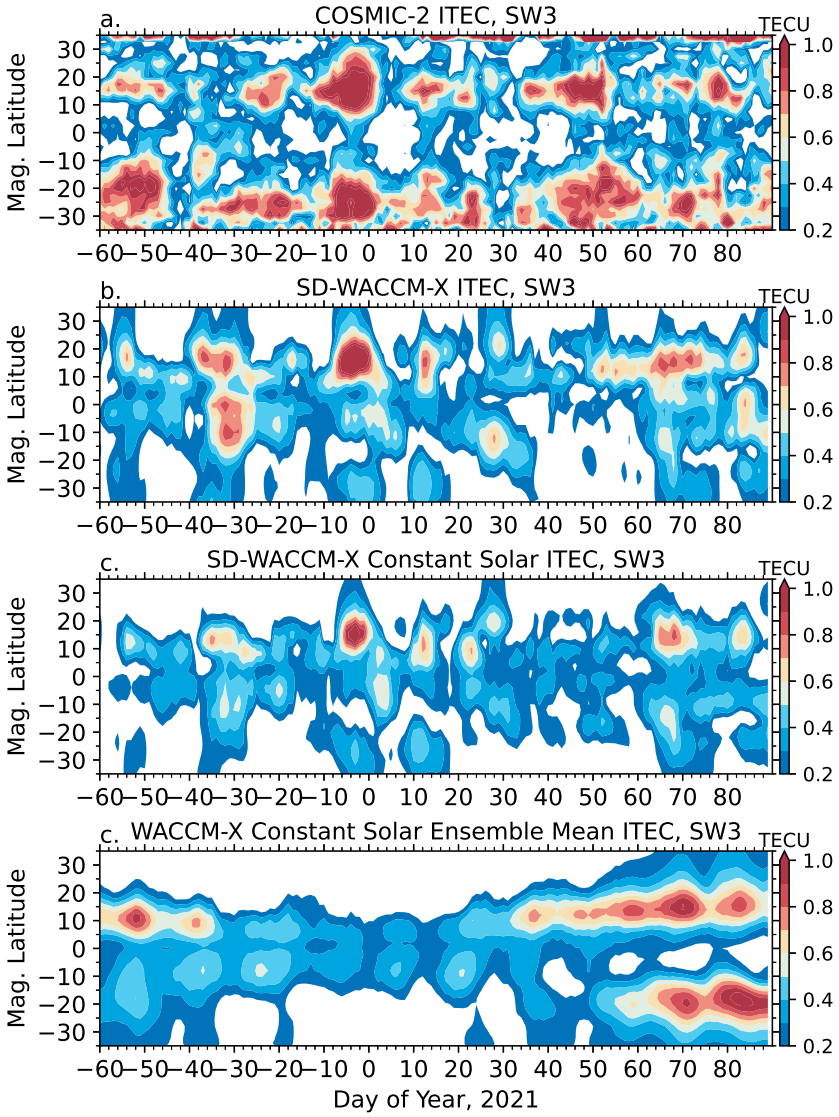

Figure 7. SW3 amplitude in ITEC from (**a**) COSMIC-2 observations, (**b**) SD-WACCM-X, (**c**) SD-WACCM-X Constant Solar, and (**d**) WACCM-X Constant Solar Ensemble Mean.

4. Summary and Conclusions

The impact of the 2020–2021 SSW on the low latitude ionosphere was demonstrated in the present study using a combination of COSMIC-2 observations and WACCM-X simulations. This represents the first global-scale observational investigation into the short-term ionosphere variability during a SSW event and was enabled by the dense sampling of the low latitude ionosphere provided by COSMIC-2. The COSMIC-2 observations revealed that several notable changes occurred in the ionosphere during the 2020–2021 SSW. By combining the observations with WACCM-X simulations, the observed variability can be separated into variability driven by geomagnetic/solar activity and that due to the SSW. SSW induced changes in the ionosphere observed by COSMIC-2 include:

1. A ∼20 day decrease in the zonal and diurnal average ITEC beginning around the SSW onset in early January 2021. This decrease is attributed to changes in the residual circulation in the MLT, which altered the mean composition of the thermosphere and ionosphere.

2. A decrease in the diurnal amplitude (i.e., DW1) in the ionosphere in early January. The decreased diurnal variability in the ionosphere was coincident, and connected to, the decreased zonal and diurnal average ITEC.

3. An increase in the ITEC SW2, which was a combination of the solar and lunar semidiurnal migrating tides, during the SSW that was attributed to the influence of enhanced SW2 amplitudes in the MLT on the electrodynamics of the low latitude ionosphere.

4. Periodic enhancements occurred in the ITEC SW1, which may be due to enhanced SW1 amplitudes in the MLT. This is, however, difficult to determine due to poor agreement between the observed and simulated SW1.

5. Enhanced ITEC SW3 amplitudes ∼10 days before and ∼5 days after the SSW onset. These enhancements are thought to be due to nonlinear planetary wave–tide interactions that led to enhanced SW3 amplitudes in the MLT at these times.

From these results, it is clearly evident that the 2020–2021 SSW significantly impacted the low latitude ionosphere electron densities, and, most likely, also the electrodynamics. Furthermore, they demonstrate the unique capabilities of the COSMIC-2 observations to investigate the day-to-day variability of the low latitude ionosphere that arises due to lower atmosphere meteorological variability.

Funding: This research was funded by the National Aeronautics and Space Administration (NASA) Heliophysics Supporting Research Grant 80NSSC18K1046 and National Science Foundation (NSF) Grant AGS-2054356. These results are partly based upon work supported by the National Center for Atmospheric Research, which is a major facility sponsored by the National Science Foundation under Cooperative Agreement No. 1852977.

Institutional Review Board Statement: Not applicable.

Informed Consent Statement: Not applicable.

Data Availability Statement: COSMIC-2 electron density profiles are available via the COSMIC Data Analysis and Archive Center (https://doi.org/10.5065/t353-c093, accessed on 23 January 2022). The Community Earth System Model (CESM), including WACCM-X, is available from https://www.cesm.ucar.edu/ (accessed 4 October 2019). Numerical simulation output for the SD-WACCM-X (https://doi.org/10.5281/zenodo.5884908, accessed on 23 January 2022), SD-WACCM-X Constant Solar (https://doi.org/10.5281/zenodo.5884943, accessed on 23 January 2022), and WACCM-X Constant Solar Ensemble Mean (https://doi.org/10.5281/zenodo.5884985, accessed on 23 January 2022) are available on Zenodo.

Acknowledgments: Computing and data storage resources, including the Cheyenne supercomputer (https://doi.org/10.5065/D6RX99HX, accessed on 23 January 2022), were provided by the Computational and Information Systems Laboratory (CISL) at NCAR.

Conflicts of Interest: The author declares no conflict of interest.

References

1. Matsuno, T. A Dynamical Model of the Stratospheric Sudden Warming. *J. Atmos. Sci.* **1971**, *28*, 1479–1494. [CrossRef]
2. Charlton, A.J.; Polvani, L.M. A New Look at Stratospheric Sudden Warmings. Part I: Climatology and Modeling Benchmarks. *J. Clim.* **2007**, *20*, 449–469. [CrossRef]
3. Pedatella, N.M.; Chau, J.L.; Schmidt, H.; Goncharenko, L.P.; Stolle, C.; Hocke, K.; Harvey, V.L.; Funke, B.; Siddiqui, T.A. How sudden stratospheric warming affects the whole atmosphere. *EOS* **2018**, *99*, 35–38. [CrossRef]
4. Baldwin, M.P.; Ayarzagüena, B.; Birner, T.; Butchart, N.; Butler, A.H.; Charlton-Perez, A.J.; Domeisen, D.I.V.; Garfinkel, C.I.; Garny, H.; Gerber, E.P.; et al. Sudden Stratospheric Warmings. *Rev. Geophys.* **2021**, *59*, e2020RG000708. [CrossRef]
5. Stening, R.J. Electron density profile changes associated with the equatorial electrojet. *J. Atmos. Terr. Phys.* **1977**, *39*, 157–164. [CrossRef]
6. Goncharenko, L.; Zhang, S.R. Ionospheric signatures of sudden stratospheric warming: Ion temperature at middle latitude. *Geophys. Res. Lett.* **2008**, *35*, L21103. [CrossRef]
7. Chau, J.L.; Fejer, B.G.; Goncharenko, L.P. Quiet variability of equatorial E × B drifts during a sudden stratospheric warming event. *Geophys. Res. Lett.* **2009**, *36*, L05101. [CrossRef]
8. Goncharenko, L.P.; Chau, J.L.; Liu, H.L.; Coster, A.J. Unexpected connections between the stratosphere and ionosphere. *Geophys. Res. Lett.* **2010**, *37*, L10101. [CrossRef]
9. Chau, J.L.; Goncharenko, L.P.; Fejer, B.G.; Liu, H.L. Equatorial and Low Latitude Ionospheric Effects During Sudden Stratospheric Warming Events. *Space Sci. Rev.* **2012**, *168*, 385–417. [CrossRef]

10. Goncharenko, L.P.; Harvey, V.L.; Liu, H.; Pedatella, N.M. Sudden Stratospheric Warming Impacts on the Ionosphere–Thermosphere System. In *Ionosphere Dynamics and Applications*; American Geophysical Union (AGU): Washington, DC, USA, 2021; Chapter 16, pp. 369–400. [CrossRef]
11. Jin, H.; Miyoshi, Y.; Pancheva, D.; Mukhtarov, P.; Fujiwara, H.; Shinagawa, H. Response of migrating tides to the stratospheric sudden warming in 2009 and their effects on the ionosphere studied by a whole atmosphere-ionosphere model GAIA with COSMIC and TIMED/SABER observations. *J. Geophys. Res. Space Phys.* **2012**, *117*, A10323. [CrossRef]
12. Forbes, J.M.; Zhang, X. Lunar tide amplification during the January 2009 stratosphere warming event: Observations and theory. *J. Geophys. Res. Space Phys.* **2012**, *117*, A12312. [CrossRef]
13. Siddiqui, T.A.; Maute, A.; Pedatella, N.M. On the Importance of Interactive Ozone Chemistry in Earth-System Models for Studying Mesophere-Lower Thermosphere Tidal Changes during Sudden Stratospheric Warmings. *J. Geophys. Res. Space Phys.* **2019**, *124*, 10690–10707. [CrossRef]
14. Fang, T.W.; Fuller-Rowell, T.; Akmaev, R.; Wu, F.; Wang, H.; Anderson, D. Longitudinal variation of ionospheric vertical drifts during the 2009 sudden stratospheric warming. *J. Geophys. Res. Space Phys.* **2012**, *117*, A03324. [CrossRef]
15. Pedatella, N.M.; Richmond, A.D.; Maute, A.; Liu, H.L. Impact of semidiurnal tidal variability during SSWs on the mean state of the ionosphere and thermosphere. *J. Geophys. Res. Space Phys.* **2016**, *121*, 8077–8088. [CrossRef]
16. Oberheide, J.; Pedatella, N.M.; Gan, Q.; Kumari, K.; Burns, A.G.; Eastes, R.W. Thermospheric Composition O/N Response to an Altered Meridional Mean Circulation During Sudden Stratospheric Warmings Observed by GOLD. *Geophys. Res. Lett.* **2020**, *47*, e2019GL086313. [CrossRef]
17. Goncharenko, L.P.; Coster, A.J.; Chau, J.L.; Valladares, C.E. Impact of sudden stratospheric warmings on equatorial ionization anomaly. *J. Geophys. Res. Space Phys.* **2010**, *115*, A00G07. [CrossRef]
18. Anderson, D.; Araujo-Pradere, E.A. Sudden stratospheric warming event signatures in daytime ExB drift velocities in the Peruvian and Philippine longitude sectors for January 2003 and 2004. *J. Geophys. Res. Space Phys.* **2010**, *115*, A00G05. [CrossRef]
19. Maute, A.; Hagan, M.E.; Yudin, V.; Liu, H.L.; Yizengaw, E. Causes of the longitudinal differences in the equatorial vertical ExB drift during the 2013 SSW period as simulated by the TIME-GCM. *J. Geophys. Res. Space Phys.* **2015**, *120*, 5117–5136. [CrossRef]
20. McDonald, S.E.; Sassi, F.; Tate, J.; McCormack, J.; Kuhl, D.D.; Drob, D.P.; Metzler, C.; Mannucci, A.J. Impact of non-migrating tides on the low latitude ionosphere during a sudden stratospheric warming event in January 2010. *J. Atmos. Solar-Terrestrial Phys.* **2018**, *171*, 188–200. [CrossRef]
21. Lin, J.T.; Lin, C.H.; Chang, L.C.; Huang, H.H.; Liu, J.Y.; Chen, A.B.; Chen, C.H.; Liu, C.H. Observational evidence of ionospheric migrating tide modification during the 2009 stratospheric sudden warming. *Geophys. Res. Lett.* **2012**, *39*, L02101. [CrossRef]
22. Lin, C.H.; Lin, J.T.; Chang, L.C.; Liu, J.Y.; Chen, C.H.; Chen, W.H.; Huang, H.H.; Liu, C.H. Observations of global ionospheric responses to the 2009 stratospheric sudden warming event by FORMOSAT-3/COSMIC. *J. Geophys. Res. Space Phys.* **2012**, *117*, A06323. [CrossRef]
23. Anthes, R.A.; Schreiner, W.S. Six new satellites watch the atmosphere over Earth's equator. *EOS 100* **2019**. [CrossRef]
24. Yue, X.; Schreiner, W.S.; Pedatella, N.; Anthes, R.A.; Mannucci, A.J.; Straus, P.R.; Liu, J.Y. Space Weather Observations by GNSS Radio Occultation: From FORMOSAT-3/COSMIC to FORMOSAT-7/COSMIC-2. *Space Weather* **2014**, *12*, 616–621. [CrossRef] [PubMed]
25. Schreiner, W.S.; Sokolovskiy, S.V.; Rocken, C.; Hunt, D.C. Analysis and validation of GPS/MET radio occultation data in the ionosphere. *Radio Sci.* **1999**, *34*, 949–966. [CrossRef]
26. Cherniak, I.; Zakharenkova, I.; Braun, J.; Wu, Q.; Pedatella, N.M.; Schreiner, W.S.; Weiss, J.P.; Hunt, D.C. Accuracy Assessment of the Quiet-time Ionospheric F2 peak Parameters as Derived from COSMIC-2 multi-GNSS Radio Occultation. *J. Space Weather Space Clim.* **2021**, *11*, 18. [CrossRef]
27. Chang, L.C.; Lin, C.H.; Liu, J.Y.; Balan, N.; Yue, J.; Lin, J.T. Seasonal and local time variation of ionospheric migrating tides in 2007–2011 FORMOSAT-3/COSMIC and TIE-GCM total electron content. *J. Geophys. Res. Space Phys.* **2013**, *118*, 2545–2564. [CrossRef]
28. Pedatella, N.M.; Forbes, J.M. Evidence for stratosphere sudden warming-ionosphere coupling due to vertically propagating tides. *Geophys. Res. Lett.* **2010**, *37*, L11104. [CrossRef]
29. Lin, J.T.; Lin, C.H.; Lin, C.Y.; Pedatella, N.M.; Rajesh, P.K.; Matsuo, T.; Liu, J.Y. Revisiting the Modulations of Ionospheric Solar and Lunar Migrating Tides During the 2009 Stratospheric Sudden Warming by Using Global Ionosphere Specification. *Space Weather* **2019**, *17*, 767–777. [CrossRef]
30. Danabasoglu, G.; Lamarque, J.F.; Bacmeister, J.; Bailey, D.A.; DuVivier, A.K.; Edwards, J.; Emmons, L.K.; Fasullo, J.; Garcia, R.; Gettelman, A.; et al. The Community Earth System Model Version 2 (CESM2). *J. Adv. Model. Earth Syst.* **2020**, *12*, e2019MS001916. [CrossRef]
31. Neale, R.B.; Richter, J.; Park, S.; Lauritzen, P.H.; Vavrus, S.J.; Rasch, P.J.; Zhang, M. The Mean Climate of the Community Atmosphere Model (CAM4) in Forced SST and Fully Coupled Experiments. *J. Clim.* **2013**, *26*, 5150–5168. [CrossRef]
32. Marsh, D.R.; Mills, M.J.; Kinnison, D.E.; Lamarque, J.F.; Calvo, N.; Polvani, L.M. Climate change from 1850 to 2005 simulated in CESM1(WACCM). *J. Clim.* **2013**, *26*, 7372–7391. [CrossRef]
33. Qian, L.; Burns, A.G.; Emery, B.A.; Foster, B.; Lu, G.; Maute, A.; Richmond, A.D.; Roble, R.G.; Solomon, S.C.; Wang, W. The NCAR TIE-GCM. In *Modeling the Ionosphere-Thermosphere System*; American Geophysical Union (AGU): Washington, DC, USA, 2014; Chapter 7, pp. 73–83. [CrossRef]

34. Liu, H.L.; Bardeen, C.G.; Foster, B.T.; Lauritzen, P.; Liu, J.; Lu, G.; Marsh, D.R.; Maute, A.; McInerney, J.M.; Pedatella, N.M.; et al. Development and Validation of the Whole Atmosphere Community Climate Model With Thermosphere and Ionosphere Extension (WACCM-X 2.0). *J. Adv. Model. Earth Syst.* **2018**, *10*, 381–402. [CrossRef]
35. Liu, J.; Liu, H.; Wang, W.; Burns, A.G.; Wu, Q.; Gan, Q.; Solomon, S.C.; Marsh, D.R.; Qian, L.; Lu, G.; et al. First Results From the Ionospheric Extension of WACCM-X During the Deep Solar Minimum Year of 2008. *J. Geophys. Res. Space Phys.* **2018**, *123*, 1534–1553. [CrossRef]
36. Gelaro, R.; McCarty, W.; Suárez, M.J.; Todling, R.; Molod, A.; Takacs, L.; Randles, C.A.; Darmenov, A.; Bosilovich, M.G.; Reichle, R.; et al. The Modern-Era Retrospective Analysis for Research and Applications, Version 2 (MERRA-2). *J. Clim.* **2017**, *30*, 5419–5454. [CrossRef]
37. Smith, A.K.; Pedatella, N.M.; Marsh, D.R.; Matsuo, T. On the Dynamical Control of the Mesosphere–Lower Thermosphere by the Lower and Middle Atmosphere. *J. Atmos. Sci.* **2017**, *74*, 933–947. [CrossRef]
38. Solomon, S.C.; Qian, L. Solar extreme-ultraviolet irradiance for general circulation models. *J. Geophys. Res. Space Phys.* **2005**, *110*, A10306. [CrossRef]
39. Heelis, R.A.; Lowell, J.K.; Spiro, R.W. A model of the high-latitude ionospheric convection pattern. *J. Geophys. Res. Space Phys.* **1982**, *87*, 6339–6345. [CrossRef]
40. Emery, B.A.; Roble, R.G.; Ridley, E.C.; Richmond, A.D.; Knipp, D.J.; Crowley, G.; Evans, D.S.; Rich, F.J.; Maeda, S. *Parameterization of the Ion Convection and the Auroral Oval in the NCAR Thermospheric General Circulation Models*; Tech. Rep. No. NCAR/TN-491+STR; University Corporation for Atmospheric Research: Boulder, CO, USA, 2012. [CrossRef]
41. Pedatella, N.M.; Liu, H.L.; Richmond, A.D. Atmospheric semidiurnal lunar tide climatology simulated by the Whole Atmosphere Community Climate Model. *J. Geophys. Res. Space Phys.* **2012**, *117*, A06327. [CrossRef]
42. Rao, J.; Garfinkel, C.I.; Wu, T.; Lu, Y.; Lu, Q.; Liang, Z. The January 2021 Sudden Stratospheric Warming and Its Prediction in Subseasonal to Seasonal Models. *J. Geophys. Res. Atmos.* **2021**, *126*, e2021JD035057. [CrossRef]
43. Cai, X.; Burns, A.G.; Wang, W.; Qian, L.; Pedatella, N.; Coster, A.; Zhang, S.; Solomon, S.C.; Eastes, R.W.; Daniell, R.E.; et al. Variations in Thermosphere Composition and Ionosphere Total Electron Content Under "Geomagnetically Quiet" Conditions at Solar-Minimum. *Geophys. Res. Lett.* **2021**, *48*, e2021GL093300. [CrossRef]
44. Pancheva, D.; Mukhtarov, P.; Andonov, B. Nonmigrating tidal activity related to the sudden stratospheric warming in the Arctic winter of 2003/2004. *Ann. Geophys.* **2009**, *27*, 975–987. [CrossRef]
45. Lieberman, R.S.; Riggin, D.M.; Ortland, D.A.; Oberheide, J.; Siskind, D.E. Global observations and modeling of nonmigrating diurnal tides generated by tide-planetary wave interactions. *J. Geophys. Res. Atmos.* **2015**, *120*, 11419–11437. [CrossRef]
46. Pedatella, N.M.; Liu, H.L.; Richmond, A.D.; Maute, A.; Fang, T.W. Simulations of solar and lunar tidal variability in the mesosphere and lower thermosphere during sudden stratosphere warmings and their influence on the low-latitude ionosphere. *J. Geophys. Res. Space Phys.* **2012**, *117*, A08326. [CrossRef]
47. Pedatella, N.M.; Liu, H. The influence of atmospheric tide and planetary wave variability during sudden stratosphere warmings on the low latitude ionosphere. *J. Geophys. Res. Space Phys.* **2013**, *118*, 5333–5347. [CrossRef]
48. He, M.; Chau, J.L. Mesospheric semidiurnal tides and near-12 h waves through jointly analyzing observations of five specular meteor radars from three longitudinal sectors at boreal midlatitudes. *Atmos. Chem. Phys.* **2019**, *19*, 5993–6006. [CrossRef]
49. Pedatella, N.M.; Fuller-Rowell, T.; Wang, H.; Jin, H.; Miyoshi, Y.; Fujiwara, H.; Shinagawa, H.; Liu, H.L.; Sassi, F.; Schmidt, H.; et al. The neutral dynamics during the 2009 sudden stratosphere warming simulated by different whole atmosphere models. *J. Geophys. Res. Space Phys.* **2014**, *119*, 1306–1324. [CrossRef]
50. McLandress, C. The Seasonal Variation of the Propagating Diurnal Tide in the Mesosphere and Lower Thermosphere. Part I: The Role of Gravity Waves and Planetary Waves. *J. Atmos. Sci.* **2002**, *59*, 893–906. [CrossRef]
51. Liu, H.L.; Wang, W.; Richmond, A.D.; Roble, R.G. Ionospheric variability due to planetary waves and tides for solar minimum conditions. *J. Geophys. Res. Space Phys.* **2010**, *115*, A00G01. [CrossRef]
52. Maute, A.; Hagan, M.E.; Richmond, A.D.; Roble, R.G. TIME-GCM study of the ionospheric equatorial vertical drift changes during the 2006 stratospheric sudden warming. *J. Geophys. Res. Space Phys.* **2014**, *119*, 1287–1305. [CrossRef]
53. Millward, G.H.; Müller-Wodarg, I.C.F.; Aylward, A.D.; Fuller-Rowell, T.J.; Richmond, A.D.; Moffett, R.J. An investigation into the influence of tidal forcing on F region equatorial vertical ion drift using a global ionosphere-thermosphere model with coupled electrodynamics. *J. Geophys. Res. Space Phys.* **2001**, *106*, 24733–24744. [CrossRef]
54. Liu, H.L.; Richmond, A.D. Attribution of ionospheric vertical plasma drift perturbations to large-scale waves and the dependence on solar activity. *J. Geophys. Res. Space Phys.* **2013**, *118*, 2452–2465. [CrossRef]